Integrative Biology

Cite this: *Integr. Biol.*, 2012, **4**, 1540–1549

www.rsc.org/ibiology

TECHNICAL INNOVATION

Responsive culture platform to examine the influence of microenvironmental geometry on cell function in 3D

April M. Kloxin,†‡[a] Katherine J. R. Lewis,‡[a] Cole A. DeForest,§[a] Gregory Seedorf,[b] Mark W. Tibbitt,[a] Vivek Balasubramaniam[b] and Kristi S. Anseth*[acd]

Received 5th September 2012, Accepted 27th October 2012
DOI: 10.1039/c2ib20212c

We describe the development of a well-based cell culture platform that enables experimenters to control the geometry and connectivity of cellular microenvironments spatiotemporally. The base material is a hydrogel comprised of photolabile and enzyme-labile crosslinks and pendant cell adhesion sequences, enabling spatially-specific, *in situ* patterning with light and cell-dictated microenvironment remodeling through enzyme secretion. Arrays of culture wells of varying shape and size were patterned into the hydrogel surface using photolithography, where well depth was correlated with irradiation dose. The geometry of these devices can be subsequently modified through sequential patterning, while simultaneously monitoring changes in cell geometry and connectivity. Towards establishing the utility of these devices for dynamic evaluation of the influence of physical cues on tissue morphogenesis, the effect of well shape on lung epithelial cell differentiation (*i.e.*, primary mouse alveolar type II cells, ATII cells) was assessed. Shapes inspired by alveoli were degraded into hydrogel surfaces. ATII cells were seeded within the well-based arrays and encapsulated by the addition of a top hydrogel layer. Cell differentiation in response to these geometries was characterized over 7 days of culture with immunocytochemistry (surfactant protein C, ATII; T1α protein, alveolar type I (ATI) differentiated epithelial cells) and confocal image analysis. Individual cell clusters were further connected by eroding channels between wells during culture *via* controlled two-photon irradiation. Collectively, these studies demonstrate the development and utility of responsive hydrogel culture devices to study how a range of microenvironment geometries of evolving shape and connectivity might influence or direct cell function.

[a] *Chemical and Biological Engineering, University of Colorado, Boulder, CO, USA. E-mail: kristi.anseth@colorado.edu; Tel: +1 (303)-735-5336*
[b] *Pediatric Heart Lung Center Laboratory, University of Colorado, Denver, CO, USA*
[c] *Howard Hughes Medical Institute, University of Colorado, Boulder, CO, USA*
[d] *BioFrontiers Institute, University of Colorado, Boulder, CO, USA*
† Current address: Chemical & Biomolecular Engineering and Materials Science & Engineering, University of Delaware, Newark, DE, USA.
‡ These authors made equal contributions to this work.
§ Current address: Chemistry & Chemical Engineering, California Institute of Technology, Pasadena, CA, USA.

Introduction

Extracellular matrix (ECM) signals, such as elasticity,[1] growth factor presentation,[2] and extracellular matrix protein assembly and binding,[3] are increasingly recognized as critical regulators of progenitor cell function and fate during development and tissue regeneration. For example, during lung development, spatiotemporally evolving growth factor gradients, basement membrane production and localized remodeling, and interactions between adjacent cells responding to the locally thinned and distended basement membrane are all part of the complex

Insight, innovation, integration

This paper reports a well-defined platform to control cell cluster shape dynamically during 3D culture, facilitating unique experiments of how microenvironment geometry and connectivity influence cell function and fate. A photolabile, enzyme-labile hydrogel was fabricated to enable *in situ*, spatially-specific property modulation and cell response assessment. Within this synthetic extracellular matrix, an array of culture wells with varying shape and size was created by photodegradation *via* photolithography. The utility of these devices for dynamic cell culture was demonstrated with lung epithelial cells, where the influence of alveolar-inspired shapes on epithelial cell differentiation was investigated. This platform can be used to study how a range of microenvironment geometries with evolving shapes or connectivities influence cell fate in tissue morphogenesis or regeneration.

sequence of ECM signals that direct lung epithelium assembly, branching morphogenesis, and alveoli formation.[4] In particular, the geometry of the cell microenvironment, which regulates cell shape and cytoskeletal tension, polarization, receptor binding, and cell–cell communication,[4c,5] in conjunction with biochemical factors, has been observed to direct cell differentiation and function in both tissue regeneration[6] and morphogenesis.[7] While many studies have demonstrated the importance of microenvironment geometry in guiding cell function within these biological processes, the native cell microenvironment contains a complex array of biophysical and biochemical signals that actively and reciprocally interact with cells.[8] A culture platform that more fully captures changes in microenvironment geometry in three dimensions would be useful to understand the transient role of cell shape in tissue development or regeneration. Here, we present a new culture platform based on photodegradable materials for spatiotemporally controlling cell geometry during culture and demonstrate its utility for probing the role of shape in influencing progenitor cell fate, specifically alveolar type II (ATII) epithelial cell differentiation.

Cell microenvironment geometry has been controlled *in vitro* with micropatterned culture substrates. Both hard and soft materials have been patterned to control cell adhesion and shape within two-dimensional (2D) culture,[5,9] where shape has been observed to regulate cell differentiation and fate.[6a,10] Culture platforms that mimic native tissue geometry and architecture in three dimensions can be advantageous for recapturing *in vivo*-like cell response.[11] To control microenvironment geometry in three-dimensional (3D) culture, micropatterned well-based materials have been developed and utilized to examine mammary branching morphogenesis,[7b,12] the epithelial–mesenchymal transition,[13] and MSC differentiation.[14] These well-based culture platforms are created using soft lithography to pattern arrays of wells within collagen hydrogels:[15] a PDMS stamp with 50–100 μm tall circular or rectangular posts is typically embedded within a liquid collagen mixture; the collagen mixture is crosslinked; and the stamp is removed, generating wells in which cells of interest are seeded. Subsequently, a second layer of collagen is added to encapsulate the cells within a spatially-defined 3D microenvironment. Cell function and fate in these micropatterned geometries are assessed using biochemical assays to quantify cell proliferation, apoptosis, or protein production and immunocytochemistry to examine cell phenotype, morphology and cytoskeletal organization, or cell–ECM/cell–cell interactions. In complementary approaches, 3D culture of cell aggregates has been achieved by using microwells and microengineering[16] or using micropatterning and electromagnetic fields to orient cell aggregates followed by photoencapsulation within a 3D polymer matrix.[17]

From these seminal contributions, the importance of 3D culture for examining the complex signaling involved in whole tissue development or regeneration is clearly demonstrated. Cytoskeletal tension in conjunction with cell-secreted factors, cell–cell interactions, and cell–ECM binding has been observed to regulate morphogenesis in ECM–protein-based culture systems. Further, the relevant size and time scales for a geometrically defined 3D culture system have been identified, with geometries ranging from 50–250 μm in width for cylinders, rectangular prisms, and cubes while assessing cell fate decisions from days to weeks.[7]

A 3D culture platform that enables similar studies with temporally-evolving biophysical signals would offer further insight into the critical cues and mechanisms that drive tissue development and repair. The culture platform should afford (i) ease of handling throughout cell culture, (ii) accessible, facile generation of an array of microenvironment geometries, (iii) *in situ* biological assays for spatially-specific assessment of cell response, and (iv) spatiotemporal property manipulation to elucidate how evolving microenvironment geometry/connectivity influence cell fate.

In this contribution, we exploit a relatively unique and photodegradable material system by processing it into a microfabricated culture system and then studying how geometry temporally regulates lung epithelial cell function and fate. Inspired by prior 3D well-based culture platforms, we developed an approach for preparing devices with arrays of wells with varied shape and size and subsequently utilized them for 3D cell culture by seeding, encapsulation, and assessment of cells within the controlled shapes. A photolabile and enzymatically-degradable hydrogel was employed as the device foundation, and this base material was modified with integrin-binding peptides to promote cell adhesion and serve as an artificial, well-defined ECM. The photolabile functionality uniquely allowed the formation and later modification of well shapes, while the enzyme cleavage sites allowed cell-based remodeling of the matrix during long-term culture. Well shape, depth, and connectivity were controlled with photolithography or focused two-photon irradiation using a confocal microscope. With this platform, we examined how geometry influences ATII epithelial cell fate, where ATIIs are the progenitor cells for both ATII and ATI cell populations in the alveolar epithelium.[18] In the native lung, ATII cells are also responsible for surfactant production and secretion, whereas ATI cells cover most of the alveolar surface area and promote gas exchange. Alveoli-inspired shapes were facilely created using photolithography, and cell phenotype in response to these geometries was characterized with *in situ* immunocytochemistry and confocal microscopy. The cell-laden wells were connected with channels by controlled photodegradation during culture to mimic branching and connectivity. This device system based on dynamically controlled hydrogel materials should prove useful for probing how many cell types respond to changes in microenvironment geometry and improve the field's understanding of the role of physical cues in directing tissue morphogenesis or regeneration.

Materials and methods

All reagents were purchased from Sigma Aldrich and used as received unless otherwise noted.

Synthesis of responsive monomers

A photolabile, enzyme-labile peptide functionalized with azides, N_3-RGK(alloc)GPQG↓IWGQRK(PL-ester-N_3)-NH_2, was synthesized according to previously published methods.[19] An *o*-nitrobenzyl ether photolabile group was incorporated to allow cleavage with externally-applied UV, visible, and two-photon irradiation.[20] A synthetic variant of an enzymatically

degradable peptide sequence from collagen I was incorporated to allow directed degradation by many different cell types with a host of secreted matrix metalloproteinases (MMPs), including MMPs 1, 2, 3, 8, and 9.[21] A multi-arm poly(ethylene glycol) (M_n ~ 10 kDa, JenKem Technology USA) modified with cyclooctyne end groups was synthesized according to previously published methods.[22] An azide-modified carboxylic acid was synthesized using previously published techniques[22] for subsequent attachment to amine-modified glass, as described in the following section.

Fabrication of hydrogel culture platform

Glass cover slips (#2; 22, or 18 mm diameter; Fisher Scientific) were cleaned with Piranha (30 min in freshly prepared 3 : 1 by volume concentrated sulfuric acid to 30% hydrogen peroxide solution, Fisher Scientific) rinsed with copious amounts of deionized water (DI) water, using appropriate safety precautions and personal protective equipment. After all Piranha waste was removed from the fume hood, the clean cover glass was rinsed with acetone and allowed to dry in the fume hood. This glass was modified with an amino-silane ((3-aminopropyl)-triethoxysilane, Gelest) based on a modified version of a published protocol.[23] Briefly, glass slides were immersed in 70 mM (3-aminopropyl)-triethoxysilane and 70 mM *n*-butyl amine in toluene and allowed to react 90 minutes at room temperature. They were then wiped with a toluene-wet kimwipe and dried overnight in an 80 °C oven. The amine-functionalized glass was subsequently reacted with the azide-modified carboxylic acid by immersing in 100 mM azide-butanoic acid, 100 mM HATU (ester activating agent, AnaSpec), and 100 mM *N*,*N*-diisopropylethylamine in dimethylformamide, reacting for 4^+ hours, rinsing with acetone and wiping dry, creating a thin, easy-to-handle base for hydrogel formation, patterning, and controlled cell culture. These azide-functionalized cover slides were kept at 4 °C in the dark until their use in hydrogel formation (typically used within 1 month of preparation).

Molds for hydrogel formation were assembled with an azide-functionalized cover slip, a 0.5 mm-thick, ~1 mm wide silicon rubber gasket on each side of this cover slip, and a cover slip treated with an anti-adhesion agent (Rain-X) placed offset by ~1 mm on top, creating a ~15 mm × 15 mm area with two open sides for easy addition of the liquid monomer solution.

Monomer stock solutions were prepared under sterile conditions using sterile reagents: (1) 12.5 mM PEG-tetracyclooctyne in PBS (freshly prepared, containing 50 mM difluorinated cyclooctyne ($DIFO_3$)), (2) 25 mM azide-RGDS in PBS, and (3) 24 mM bis(azide)-functionalized peptide (containing 48 mM azide) dissolved first in minimal DMSO and diluted with PBS and azide-RGDS stock solution for 2 mM RGDS (typically 1 : 5 to 1 : 10 DMSO : PBS) (freshly prepared, containing 50 mM total azide). Note that these molar concentrations (mM) assume that the contribution of the solid to the solution volume is minimal upon dissolution. The sterile Dulbecco's phosphate buffered saline (PBS, Invitrogen) contained antibiotic (50 U mL^{-1} penicillin and 50 μg mL^{-1} streptomycin, Invitrogen) and antifungal (1 μg mL^{-1} amphotericin B, Invitrogen) agents. The final gel-forming solution was comprised of equal volumes of stock solution 1 and 3 for 6.7 wt% total monomer consisting of four-arm PEG-tetracyclooctyne in PBS, bis(azide)-functionalized peptide, and 1 mM azide-RGDS (total 25 mM $DIFO_3$ and 25 mM azide). For samples whose patterning would be characterized with confocal imaging, a small amount of azide-functionalized dye stock solution was added to the gel-forming monomer solution in place of PBS (Alexa Fluor® 594 Carboxamido-(6-Azidohexanyl), Invitrogen, dissolved per manufacturer instructions) for a final concentration of 0.1 mM within the hydrogels.

The mixed monomer solution was quickly centrifuged (Mini Centrifuge, Fisher Scientific) for ~15 s to remove air bubbles, and ~50 μL of gel-forming solution was pipetted into each mold. Owing to the fast reactivity of the copper-free click chemistry, no more than ~8 samples were prepared in parallel from a single Eppendorf tube, *i.e.*, additional tubes of monomer solutions could be mixed serially to achieve the desired number of samples for an experiment. Hydrogels were allowed to polymerize in the dark for ~1 h, a time previously determined to allow complete polymerization.[19] Sterile PBS (with antifungal and antibiotic agents) was injected (26 gauge needle and syringe, BD) within the empty space surrounding the fully-formed gels, and the molds were fully submerged within a petri dish containing sterile PBS. The hydrogels were allowed to swell in this solution for 1 h, and the top Rain-X-treated cover slip was gently and carefully removed using a razor blade. The hydrogels were transferred to sterile 6-well plates, covered with fresh sterile PBS, sealed with Parafilm®, and stored at 4 °C overnight to allow any unreacted monomer to diffuse out.

Patterning of hydrogel devices

Photomasks were designed in Adobe Illustrator and emulsion printed on Mylar (Advance Reproductions, North Andover, MA). Shapes consisted of 200 μm diameter circles (Circle), two connected 100 μm diameter circles (Di), and four connected 100 μm diameter circles (Quad). Photomasks were bonded to glass slides (50 mm × 75 mm, Fisher Scientific) with the photopolymerization of a thin layer of urethane diacrylate and triethylene glycol diacrylate with I184 as the initiator to create an optically clear adhesive (40 mW cm^{-2} of 320–500 nm irradiation centered at 365 nm for 15 min, mask aligner with collimated flood exposure source, Optical Associates, Inc., San Jose, CA).[24] Wells were photodegraded into the gels by placing a gasket around the gel coverslip, covering with sterile PBS, placing the photomask slide on top of the gasket, and irradiating with collimated 365 nm light at 9 ± 1 mW cm^{-2} for up to 30 min (20 min irradiation used to pattern devices for cell seeding experiments; Omnicure S1000 with 365 nm filter, liquid filled light guide, and collimating lens, EXFO).[20g] Patterned gels were placed in sterile 12-well plates and swollen in sterile PBS containing antibiotics and antifungal overnight at 37 °C. Depths of the resulting wells were verified with profilometry (Stylus Profiler, Dektak 6M) and confocal microscopy (Zeiss 710, 10–20× water immersion objectives).[25] Irradiation intensities for all experiments were measured with a calibrated radiometer (Model IL1400A, International Light, Inc., Newburyport, MA).

Modeling of hydrogel patterning

A statistical-kinetic model of photodegradation recently was adapted to predict the depth of patterned features in these step growth hydrogels as a function of irradiation time.[25a,26] The statistical-kinetic model accounted for the attenuation of light in the sample during irradiation, the kinetics of the photocleavage of the *o*-nitrobenzyl ether (NBE) moiety, reverse gelation of the hydrogel network, and diffusion of the degraded products after reverse gelation. Briefly, the Beer–Lambert Law and a first-order expression of the photocleavage reaction were solved numerically in 1-D over the space and time of the irradiation during patterning. The probability that a NBE moiety has been cleaved was solved at each point in space and time, $P(z,t) = 1 - [\mathrm{NBE}]/[\mathrm{NBE}]_0$. When $P(z,t) \geq P_{rg} = 0.67$, the critical extent of cleavage to induce reverse gelation based on the Flory–Rehner equation,[27] it was assumed that the gel disassembled into soluble components that diffused one-dimensionally, removing attenuators of the light from the light path. By numerically solving this system of equations using finite element methods (MATLAB, MathWorks®), the erosion depth as a function of time was predicted for this hydrogel system from $t = 0$ to 30 min. The diffusion coefficient for the degraded products was assumed to be 1×10^{-6} cm^2 s^{-1} based on predicted hydrodynamic radii. The kinetic constant for photodegradation was taken from a previous analysis of the photolabile azide moiety.[19]

Cell isolation and expansion

Adenocarcinomic human alveolar basal epithelial cells (A549, ATCC) were used as a model lung epithelial cell to characterize cell seeding. A549 cells cultured per standard protocols in growth media (Dulbecco's modified Eagle's medium (DMEM), 10% fetal bovine serum (FBS), 2% penicillin/streptomycin (100 U mL^{-1}), 0.4% fungizone (0.5 μg mL^{-1}), Invitrogen) at 37 °C with 5% CO_2 and successively passaged until use in experiments. To characterize cell seeding within the devices, plated A549s (~80% confluent) were labeled with Cell Tracker Green (CTG, Invitrogen) per the manufacturer's instructions using a minimal amount of 10 μM CTG in serum free media for 30 min during the labeling step. CTG labeled A549s were used immediately in cell seeding experiments.

Alveolar type II cell (AT2) isolation

Mice (6–8 weeks old) were euthanized by CO_2 asphyxiation. The thorax was opened and the pulmonary circulation flushed with sterile PBS. The lungs were excised and distal lung tissue was minced finely and digested in 1% collagenase (Worthington Biochemical, NJ) + 1 mg ml^{-1} DNase (GIBCO BRL, Carlsbad CA) for 30 minutes. An equal volume of 2 mg ml^{-1} trypsin inhibitor (GIBCO BRL) + 2 mg ml^{-1} DNase was added and cell suspension was filtered through 10 μm pore diameter Nitex Filter. Cells were centrifuged at 430 × *g* for 10 minutes at room air temperature. Cell pellet was washed with DMEM/F12 media and plated on non-tissue culture plates coated with IgG (6 mg cm^{-2}, Sigma) for one hour at 37 °C. Non-adherent cells were recovered and centrifuged at 430 × *g* for 10 minutes. Cell pellet was resuspended and cultured in DMEM/F12 + 10% FBS.

Study animals and protocols

All procedures and protocols were reviewed and approved by the Animal Care and Use Committee at the University of Colorado Denver Anschutz Medical Campus. Mice were obtained from The Jackson Laboratories and bred in-house.

Cell seeding and encapsulation within culture platform

To characterize the relationship between cell number and seeding density, CTG-labeled A549s were trypsinized, centrifuged (1000 rpm for 5 min), and suspended at varying concentrations in growth medium (0.25 to 2.5 × 10^6 cells per mL). Cells were seeded per a modified version of previously published protocols.[14a,28] Growth medium was added to the patterned gels (1 gel per well of 12-well plate) and centrifuged at 3200 rpm for 1.5 minutes to force liquid into the wells. 2 mL of the cell suspension (0.5 to 5 × 10^6 cells per well) was added to each gel, followed by centrifugation at 1200 rpm for 2.5 minutes, rotation of the plate, and centrifugation at 1200 rpm for another 2.5 minutes. Plates were placed on an orbital shaker for 2 hours at 35 rpm and 37 °C. Media was changed and the cell-filled gels were incubated overnight.

For lung epithelial differentiation studies, freshly isolated primary adult mouse ATII cells (98–99% purity) were suspended at 1 × 10^6 cells per mL in DMEM containing 10% fetal bovine serum (FBS), antibiotic, and antimitotic. Media was added to the patterned gels and centrifuged at 3200 rpm for 1.5 minutes to force liquid into the wells. 2 mL of the cell suspension was added to each gel, followed by centrifugation at 1200 rpm for 2.5 minutes, rotation of the plate, and centrifugation at 1200 rpm for another 2.5 minutes. Plates were placed on an orbital shaker for 2 hours at 35 rpm and 37 °C. Media was changed, and the cell-filled gels were incubated overnight.

The next day, a second hydrogel layer was formed on top of the cell-seeded construct to encapsulate cells within individual wells. Media was removed from each sample. Monomer solutions were prepared as above. For each device, 25 μL of total monomer solution was mixed and allowed to react for 1 minute to increase the viscosity before adding it to the top of each cell-laden gel. In this manner, the infiltration of the top gel down into the wells was reduced creating a cell and medium filled microwell in which cells experience matrix interactions at the periphery and cell–cell interactions within the aggregate. Samples were then allowed to fully polymerize for 20 minutes at 37 °C. To remove any unreacted monomer, media was added to each sample, incubated 1 hour, and then replaced with fresh media. This was considered day 0. Encapsulated cell clusters were cultured within these devices for up to 2 weeks. Culture medium contained FGF-7 (10 ng mL^{-1}) and FGF-10 (50 ng mL^{-1}) to promote proliferation and branching, respectively.[29] Culture medium was replaced daily.

Cell response assessment

Devices were harvested at time points of interest to observe cell morphology and cell phenotype. The devices were transferred to a new 12-well plate and fixed with 4% paraformaldehyde (PFA) in PBS for 15 min at room temperature (freshly diluted from 16% PFA stock, 1 mL per sample, Electron Microscopy

Sciences), rinsed with PBS (3× of 2 mL per sample, gently rocking, 5 min), and stored in fresh PBS at 4 °C until samples for all time points were ready for staining.

Cells within the devices were labeled using immunocytochemistry for pro-surfactant protein C (an ATII cell marker in cell cytosol and secreted), T1-alpha protein (an ATI cell marker in the cell membrane), and DNA. After all samples were collected, fixed cells within devices were permeabilized in 1% TritonX-100 for 1 hour at room temperature. The samples were blocked with 40% goat serum (Invitrogen) in PBS overnight. Primary antibodies, rabbit anti-prosurfactant protein C (SPC, 1 : 100, Millipore AB3786) and hamster anti-mouse podoplanin (T1α, 1 : 100, eBioscience 14-5381-82), were added to samples with 5% polyvinylpyrrolidone (M_w 10 000 g mol^{-1}), 0.3% Tween 20, and 10% goat serum in PBS and rocked overnight. Samples were rinsed, and then incubated with secondary antibodies, goat anti-rabbit Alexa594 (1 : 200, Invitrogen) and goat anti-hamster Alexa488 (1 : 200, Invitrogen), in 4% goat serum, 0.1% Tween 20, and 0.1% bovine serum albumin in PBS for 16 hours. Samples were washed, followed by nuclei staining with DAPI (1 : 2000, Invitrogen) in PBS for 1 hour. The samples were washed with PBS twice before imaging.

All samples were imaged on a 710 LSM confocal microscope (Zeiss) with a 20× or 10× water immersion objective (NA = 1.0, Plan-Apochromat). Individual wells were centered in the imaging area and imaged from the top of the well down to the last visible cell with a *z*-stack slice step of 5 μm. Image analysis was done in Image J (NIH).

Frequency map generation

Based on an established protocol,[15] *z*-stack fluorescent images of each channel for each well were projected onto one image and converted to binary. These black-and-white images were added together to create a gray-scale image, and a HeatMap Histogram plugin (Authors: S. Pèan and M. Austenfeld, modified by K. Lewis) was used to convert the gray-scale image to a color-coded image (n = 30 wells for each frequency map).

For side-view frequency maps, ZEN software with 3D rendering was used to slice through the middle of each well in the *xz*-plane and create a composite image of half the well. The same procedure was used to create frequency maps as described above.

In situ microenvironment modification during controlled cell culture

On day 4, rectangular channels were patterned between neighboring wells using two-photon techniques where a user-defined region within the hydrogel was selectively exposed to pulsed laser light (λ = 740 nm, 5 channels per sample, approximately 400 μm × 80 μm × 90 μm). Degraded monomer was removed by swelling in fresh media. These samples were then incubated until day 7, when they were fixed and immunostained with the static culture, unmodified samples.

Results and discussion

We present the development of a culture platform that allows the experimenter to dictate the cell microenvironment geometry or connectivity and demonstrate its utility for controlled culture of lung epithelial cells (Fig. 1). The photolabile and enzyme-labile hydrogel base material enables the creation of a wide range of well depths (50 to 200$^+$ μm) and shapes using standard photolithographic techniques. Cells of interest can be facilely seeded within these wells and encapsulated to probe their response to a geometrically-defined environment, which is easily assessed with imaging-based assays. As the patterning material can be degraded by cell-secreted proteases, cells can respond to and remodel their surrounding matrix. Further, the user can initiate changes to microenvironment shape or connectivity of the cell-laden wells through controlled,

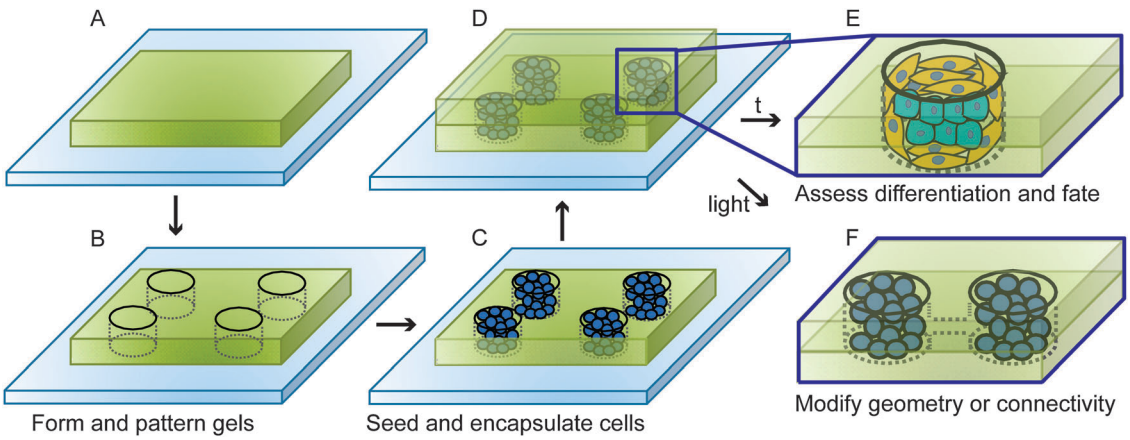

Fig. 1 Platform fabrication for dynamic control of cell cluster shape and connectivity. (A) The photolabile, enzyme-labile hydrogel base material was formed on glass cover slips to enable ease of handling for subsequent patterning or cell seeding. (B) Hydrogel layers 0.5 mm in thickness were formed to enable the stable creation of a wide range of well depths (50 to 200 μm) and shapes with photolithography. (C) These wells were seeded with cells of interest, which could be used at this point in processing for microwell cultures, and (D) a second hydrogel layer was added to encapsulate cell clusters within 3D microenvironments that enable spatiotemporally controlled geometry. (E) Cell response to their geometrically-defined environments and cell-dictated remodeling was monitored over time with live or static imaging techniques, and (F) the geometry or connectivity of the local matrix was modified at any position and time during culture with the application of cytocompatible light.

cytocompatible irradiation. We demonstrate the utility of these devices by examining how geometry regulates alveolar type II (ATII) epithelial cell fate. The versatile cell culture devices presented are a new tool for asking how geometry and connectivity dynamically regulate cell function and fate.

The base material for these devices is a light and enzyme degradable PEG hydrogel. The crosslinking monomer is a multi-arm PEG (4 arm, $M_n \sim 10$ kDa) modified with cyclooctyne end groups (Fig. 2). A photolabile, enzyme-labile peptide functionalized with azides[19] was designed to allow cleavage either by externally-applied UV, visible, and two-photon irradiation or by cell-secreted matrix metalloproteinases, including MMPs 1, 2, 3, 8, and 9.[21] These MMPs are secreted or present on the membranes of many cell types,[21c] including ATII cells which have been observed to secrete collagenase (MMP-1), gelatinase A (MMP-2), and gelatinase B (MMP-9) during *in vitro* culture.[30] Further, this enzymatically-degradable sequence derived from collagen I has been used within hydrogels for 3D culture of many cell types, including human dermal fibroblasts,[31] mesenchymal stem cells,[32] valvular interstitial cells,[33] osteoblast progenitor cells,[34] and smooth muscle cells.[35] Last, an integrin-binding ECM protein mimic, RGDS, functionalized on the N-terminus with an azide was added to the gel-forming monomer solution to promote general cell adhesion to the geometrically-defined synthetic ECM. This combination of chemistries allows copper-free click hydrogel formation and subsequent orthogonal light-based degradation and patterning or cell-driven enzymatic remodeling. While not shown here, the modulus of the base material can be easily manipulated by altering the weight percent of monomer in the hydrogel,[36] and biochemical moieties can be spatiotemporally added through radical-mediated photoaddition reactions of thiol-containing peptides with the allyl-protected lysine on the crosslinking peptide.[37]

One advantage of this system is the simplicity of the hydrogel patterning process, enabling the creation of wells of varied depth and shape *after* hydrogel formation. Shapes of interest on the micron scale can be drawn in a CAD or illustration program and printed onto transparent films for subsequent transfer with a low-intensity collimated light source. To demonstrate this practical approach, 200 μm circles individually, or in clusters as will be shown below, were drawn in Adobe Illustrator and the negative printed onto to a transparent film that was affixed to a microscope slide for patterning *via* photodegradation. Wells of the drawn shape were degraded into the hydrogel surface and subsequently seeded with cells (Fig. 3A). Good x–y pattern fidelity was observed, and well depth (≥ 50 μm) was controlled with irradiation time with a constant cytocompatible light intensity (9 ± 1 mW cm^{-2} at 365 nm) (Fig. 3B).

While the well depth did not increase linearly with irradiation time, this non-linear function was predicted by a statistical-kinetic model of photodegradation (Fig. 3B). The complex interplay between the attenuation of light, diffusion of degraded products, and photodegradation results in a non-linear surface erosion rate. Owing to the attenuation of light in the hydrogel, the degrading light is initially limited to the near surface region of the gel. This confines degradation, and ultimately erosion, to the surface. Upon erosion, the degraded products of the gel become soluble and begin to diffuse out of the path of the light. This exposes subsequent regions of the gel to irradiation, allowing the erosion process to penetrate through the material and generate patterns of increasing depth with irradiation time. Deviations between the statistical-kinetic model and experiment at later time points ($t = 30$ min) were likely due to slower diffusion rates in the experimental set-up than were assumed in the model, which would lead to a decreased extent of erosion. The pattern formation rate for this ideal network is rapid and occurs at much lower dosages of light than is required in similar

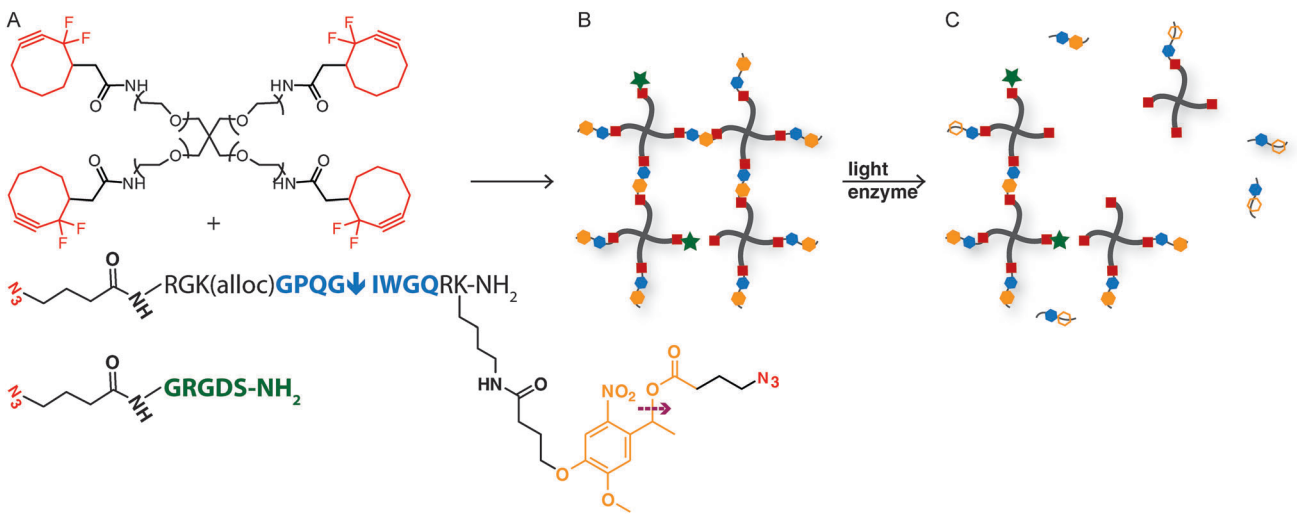

Fig. 2 Hydrogel synthesis and degradation. (A) The hydrogel base material was comprised of poly(ethylene glycol) tetracycloctyne ($M_n \sim 10$ kDa, top); photolabile, enzyme-labile, diazide peptide (middle; enzymatically cleavable sequence in blue, light cleavable moiety in yellow, cleavage positions noted by arrows); and an azide-functionalized integrin-binding adhesive ECM mimic (bottom, integrin-binding sequence in green). (B) This combination of chemistries enabled copper-free 'click', bioorthogonal hydrogel formation (C) for subsequent experimenter-initiated *in situ* photolytic patterning (cytocompatible UV, visible, and two-photon irradiation), and cell-initiated enzymatic remodeling (various MMPs including 1, 2, 3, 8, and 9).

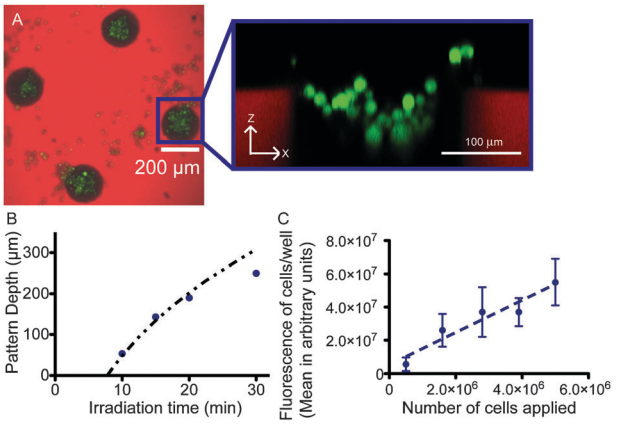

Fig. 3 Culture platform well depth and cell seeding. (A) Micron-scale wells were patterned into the surface of the hydrogel base and seeded with cells (*x*–*y* left; *x*–*z* right). (B) Well depth, measured with profilometry, was controlled predictably with irradiation time (cytocompatible $\sim 9 \pm 1$ mW cm^{-2} at 365 nm). (C) For cell seeding, a well depth of $\sim$200 μm was utilized, which was achieved with 20 min of irradiation. The total number of cells applied to each device (model lung epithelial cells, A549s, labeled with cell tracker green) linearly dictated the initial density of cells per well (measured as total green fluorescence per well). Data points are mean ± one standard deviation.

chain polymerized photodegradable hydrogels. This is advantageous not only for the rapid generation of defined patterns, but also for subsequent patterning of the gel in the presence of cells.

Cells of interest are seeded within these wells using established techniques, where cells suspended in medium at a known concentration are applied to each device and centrifuged to facilitate seeding.[28] For a given device geometry and well depth, the total number of cells applied to each device dictates the initial density of cells per well (Fig. 3C). These seeding experiments were performed with a model lung epithelial cell line (A549s labeled with cell tracker green for ease of imaging and quantification). While there is variation in cell seeding between individual wells, the overall average number of cells seeded per well is linear with the number of cells applied when averaged over the entire device ($\sim$30 wells). With a simple calibration experiment like this, the experimenter can determine the number of cells to apply to each device for the desired seeding density per well. Here, 2.75×10^6 cells per device was selected as a compromise between even well filling (see the inset Fig. 3A) and total number of cells required per experiment, which can be limited by the availability of freshly isolated primary cells. Additionally, the number of cells per device can be scaled with device surface area, where preliminary experiments were performed with devices in 6-well plates and then scaled down to the final 12-well plate size and format to conserve cells (data not shown).

We aimed to demonstrate the utility of these devices for probing the role of geometry in cell fate and focused on the hierarchically structured alveolar epithelium. Lung architecture follows an increasingly complex network of connected tubes starting from a single trachea that branches into bronchi, bronchioles, and finally ends in millions of hollow air sacs called alveoli (Fig. 4A). The major components of alveolar tissue include the single cell layer epithelium attached to the basement membrane and surrounded by a fine mesh of capillaries. There are two types of alveolar epithelial cells: ATI cells, which have an elongated morphology, form 95% of the alveolar surface area, and facilitate gas exchange between the lung and the blood stream,[38] and ATII cells, which exhibit a

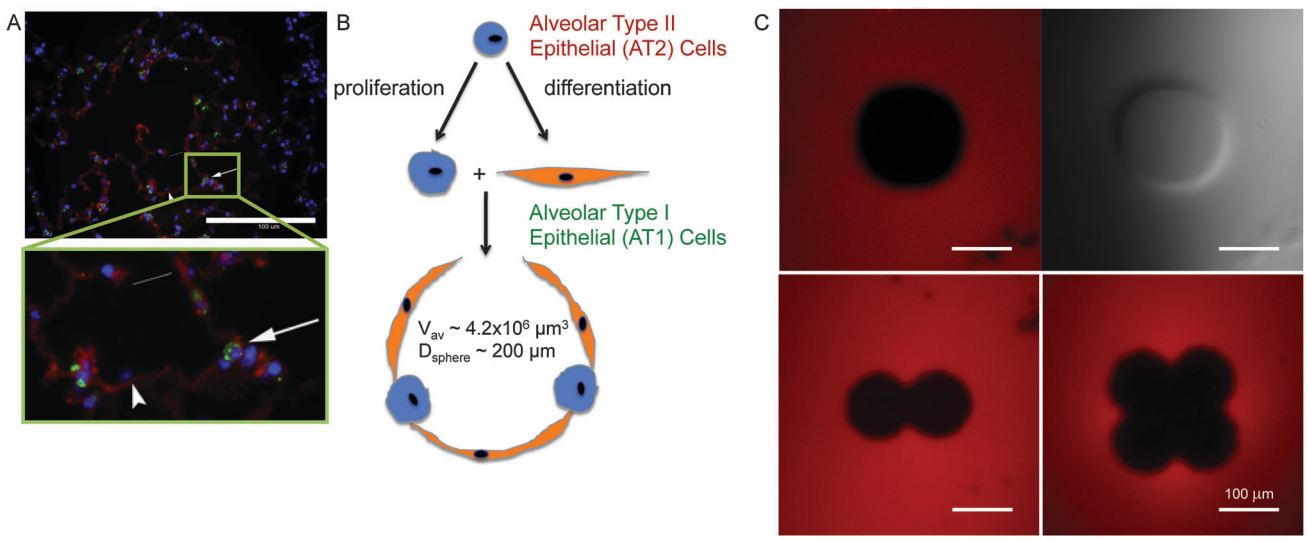

Fig. 4 Alveolar-inspired shape wells and lung epithelial cell phenotypes. (A) ATII cells (green, noted by arrows) and ATI cells (red, noted with arrowhead) comprise the alveolar epithelium (mouse lung section, blue cell nuclei, and alveolar opening noted with white line). Scale bar = 100 μm. (B) ATI cells form the barrier between the airways and the capillaries, whereas ATII cells produce lung surfactants and can proliferate and differentiate to replenish both phenotypes after injury. The volume of an adult human alveolus is estimated to be about 4.2 million cubic microns[40] which translates to a spherical diameter of about 200 μm. (C) Fluorescent and DIC images of the well shapes patterned into the gel. In this case a red fluorescent dye was incorporated into the hydrogel network so black areas are where the gel has been degraded. Given that native alveoli are not spherical, photolithographic masks were designed with an increasing number of circular lobes and an overall width of 200 μm to observe how changes in curvature affect cell fate.

cuboidal morphology, produce lung surfactants, and are the progenitor cells for both the ATII and ATI cell populations in the alveoli[18] (Fig. 4B). ATIIs are known to self renew and differentiate into ATIs during alveolar development and in response to injury; however, examining the complex milieu of signals involved in these processes *in vitro* can be difficult owing to rapid loss of the ATII phenotype during culture.[18,39]

The size and shape chosen for the wells was inspired by human alveolar geometry. The average volume for an adult human alveolus has been measured to be 4.2 million cubic microns, which corresponds to a spherical diameter of 200 microns.[40] Alveoli *in vivo*, however, are not spherical;[40,41] therefore, well shapes consisting of an increasing number of circular lobes were designed with an overall diameter of 200 microns (Fig. 4C). In native tissue, ATII cells are generally solitary and are found at the corners where neighboring alveoli meet, while ATI cells are adjacent to other ATI cells and are spread out along the curves of the alveoli.[42,43] Based on these observations, it was hypothesized that ATII phenotype cells would localize at the corners of the micropatterned wells where the curvature changes, while ATI phenotype cells would line the curved edges of the wells.

For this experiment we compared two sets of samples: one set fixed 1 day after encapsulation, and the other set fixed 7 days after encapsulation. To observe ATII differentiation within these devices, antibodies for pro-surfactant protein C (SPC, an ATII cell marker localized in the cell cytosol and potentially secreted) and T1-alpha protein (T1α, an ATI cell marker residing in the cell membrane) were used to label the two cell populations. Fluorescent images of the immunostained samples fixed on day 1 (Fig. 5A) indicate that few cells were producing T1α, the ATI cell marker, which matches expectations given that 98–99% of the cells seeded into these wells were ATII phenotypic. After 7 days T1α production was relatively high (Fig. 5B), with many elongated cells near the tops of the wells staining positive for both SPC and T1α, indicating an intermediate phenotype of alveolar epithelial cell that was transitioning from ATII to ATI. In addition, on day 7 most wells contained small, fragmented nuclei staining positive for SPC or neither marker deeper in the well, which likely maintained the ATII phenotype or were undergoing programmed cell death (apoptosis).

These initial qualitative observations were confirmed by analysis of frequency maps of SPC or T1α staining generated from 30 replicate wells of each shape (Fig. 5C). DAPI frequency maps demonstrate that cells seeded in these wells initially clustered in the center of the well during seeding and then presumably proliferated and/or migrated towards the edges to fill the well by day 7 (data not shown). As seen in Fig. 5C, after 7 days in culture SPC-positive cells tended to be located with increased frequency in the center of the well, whereas cells along the well edges tended to express T1α. These T1α-positive cells were not yet fully ATI phenotypic because they also stained positive for SPC, but given more time, they would likely continue differentiating and stop producing surfactant proteins. While in principle these experiments can be taken to longer time points, degradation of the synthetic extracellular matrix after 10 days in culture made handling of the gels during immunostaining and imaging extremely challenging and difficult to replicate.

The day 7 Quad frequency map is particularly interesting because there may have been some localization of T1α-positive cells along the inner curves of the shape. This is counter to the original hypothesis that ATII cells would prefer the corners where the curvature changes, based on lung histology. However, perhaps cells were localizing at those inner curves because they were the closest surfaces to the center of the well where the cells were initially seeded, and when the cells sensed the matrix surface, they spread out and began to differentiate. It may take additional time in culture for cells to reach the distant outer curves of the Quad shape.

By taking a cross-section of the circle wells and projecting in the y direction, frequency maps were generated to reveal the distribution in the *x*–*z* plane (Fig. 5D). Clearly, the intermediate phenotype cells staining positive for both markers reside mainly near the tops of the wells, whereas a population of ATII cells (SPC-positive only) resided primarily lower down in the wells. This observation may be relevant to normal lung tissue in which neighboring alveoli share a progenitor ATII population at the bottom of the epithelium and present the ATI cells at the top surface. The retention of the ATII cell phenotype in some cells after 7 days in culture and the vertical distribution of the differentiating and non-differentiating cell populations are reminiscent of the *in vivo* pattern. However, the aggregates in these devices do not match the exact spatial arrangement of alveolar phenotypes observed *in vivo*, which could be influenced by the lack of other lung cell types, such as fibroblasts, macrophages, and endothelial cells in the culture system. Further work will focus on the effects of the co-culture of these cell types with alveolar epithelial progenitors and the temporal and spatial effects on their growth, survival and differentiation.

Channels were successfully eroded between wells using two-photon irradiation on day 4 after encapsulation (Fig. 5E), demonstrating the ease with which matrix geometry and connectivity can be altered during cell culture. While 3T3 fibroblast cell migration has been demonstrated along channels eroded using the same techniques in equivalent gel materials,[19] almost no movement of the alveolar epithelial cells down these channels was observed by day 7. There are a few possible explanations for the absence of alveolar cell migration through these channels. RGD may be sufficient for alveolar epithelial cells to adhere to the matrix, but may not be useful for their migration, and a different peptide-based ECM mimic may be necessary for migration. Moreover, there was likely no impetus for these cells to become motile, as there was no chemical signal attracting the cells, such as a growth-factor gradient. For example, FGF-10 has been shown to be a potent chemoattractant for alveolar epithelial cells during development, and without a gradient of it, there is no lung bud outgrowth.[29b,44] The culture platform offers facile patterning of wells of varying shape, position, and connectivity at any time during cell culture, and combined with the presented quantitative imaging techniques, can be used to explore the dynamic interplay between these parameters in future experiments with alveolar epithelial cells, as well as other cell types of interest.

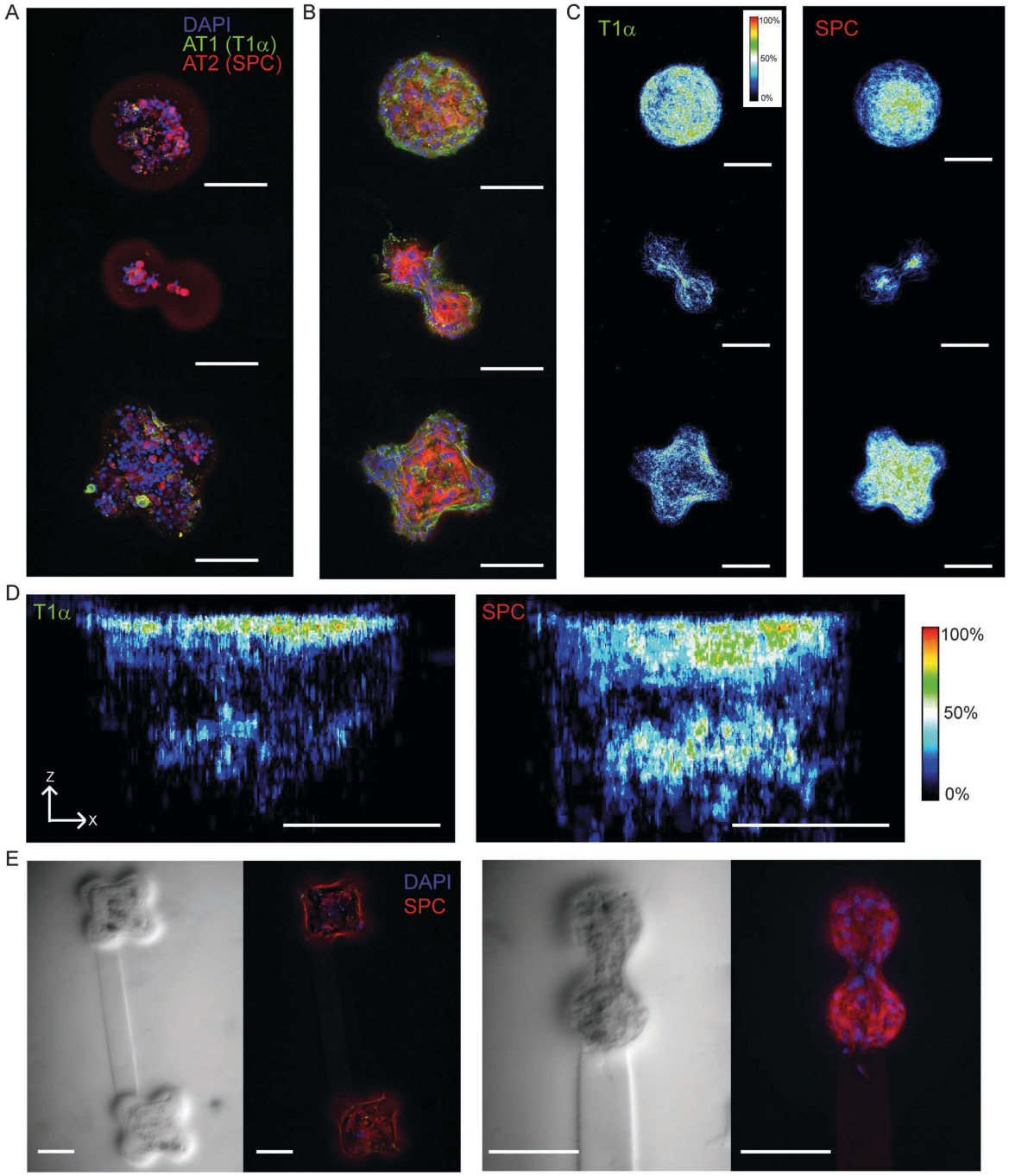

Fig. 5 Lung epithelial cell response to alveolar-inspired geometries and connectivities. (A) Representative *z*-projections of the three well shapes fixed on day 1 after encapsulation showing immunostaining for ATI cell marker (T1α), ATII cell marker (SPC), and cell nuclei (DAPI). (B) Representative *z*-projections of the three well shapes fixed on day 7 after encapsulation showing the same immunostaining as in A. (C) Frequency maps of the three well shapes showing arrangement in the *x*–*y* plane of ATI cells in the left column and of ATII cells in the right column on day 7. $n = 30$ (D) Frequency maps of a cross section of the circle wells showing arrangement in the *x*–*z* plane of ATI cells on the left and of ATII cells on the right on day 7. $n = 30$ (E) Bright field and fluorescent images of channels connecting pairs of wells patterned on day 4 after encapsulation. Samples were fixed and immunostained on day 7. All scale bars = 100 μm.

Conclusions

We have developed a dynamic, well-based cell culture platform to control the geometry and connectivity of the cell microenvironment spatiotemporally *in vitro*. Photolabile, enzyme-labile hydrogels were used as the base material, enabling the creation of wells with varied shape and depth in which primary cells were seeded and encapsulated. The utility of these devices for culturing ATII epithelial cells in defined geometries was demonstrated. This platform can be used to understand how static *or* evolving physical cues influence cell cluster shapes, cell–cell interactions, and ultimately function and fate in tissue development or regeneration.

Acknowledgements

The authors would like to thank Abigail Bernard for generously providing the urethane diacrylate and triethylene glycol diacrylate with I184 mixture for photomask adhesion and the cell seeding protocol; Balaji Sridhar for assistance with preliminary patterning and A549 seeding studies; Emily Roth, Sharon Ryan, and Liv Hoversten for assistance with preliminary A549 and ATII studies; and Ben Fairbanks for assistance with preliminary ATII 3D encapsulation studies. The authors would like to acknowledge funding from the Howard Hughes Medical Institute and NSF (DMR 1006711); M.W.T. would like to thank the Teets Family Endowed Doctoral Fellowship for funding assistance; and V.B. is supported by NIH R01 HL089262.

Notes and references

1 (*a*) D. E. Discher, P. Janmey and Y. L. Wang, *Science*, 2005, **310**, 1139; (*b*) V. Vogel and M. P. Sheetz, *Curr. Opin. Cell Biol.*, 2009, **21**, 38; (*c*) M. A. Wozniak and C. S. Chen, *Nat. Rev. Mol. Cell Biol.*, 2009, **10**, 34; (*d*) N. Wang, J. D. Tytell and D. E. Ingber, *Nat. Rev. Mol. Cell Biol.*, 2009, **10**, 75; (*e*) A. J. Keung, S. Kumar and D. V. Schaffer, in *Annual Review of Cell and Developmental Biology*, Annual Reviews: Palo Alto, 2010, vol. 26, pp. 533–556.
2 P. Tayalia and D. J. Mooney, *Adv. Mater.*, 2009, **21**, 3269.
3 (*a*) R. A. Marklein and J. A. Burdick, *Adv. Mater.*, 2010, **22**, 175; (*b*) M. P. Lutolf, P. M. Gilbert and H. M. Blau, *Nature*, 2009, **462**, 433.
4 (*a*) D. Warburton, M. Schwarz, D. Tefft, G. Flores-Delgado, K. D. Anderson and W. V. Cardoso, *Mech. Dev.*, 2000, **92**, 55; (*b*) S. Huang and D. E. Ingber, *Nat. Cell Biol.*, 1999, **1**, E131; (*c*) N. Gjorevski and C. M. Nelson, *Birth Defects Res., Part C*, 2010, **90**, 193.
5 F. Guilak, D. M. Cohen, B. T. Estes, J. M. Gimble, W. Liedtke and C. S. Chen, *Cell Stem Cell*, 2009, **5**, 17.
6 (*a*) R. McBeath, D. M. Pirone, C. M. Nelson, K. Bhadriraju and C. S. Chen, *Dev. Cell*, 2004, **6**, 483; (*b*) S. Khetan and J. A. Burdick, *Biomaterials*, 2010, **31**, 8228.
7 (*a*) C. M. Nelson, *Biochim. Biophys. Acta, Mol. Cell Res.*, 2009, **1793**, 903; (*b*) C. M. Nelson, M. M. VanDuijn, J. L. Inman, D. A. Fletcher and M. J. Bissell, *Science*, 2006, **314**, 298.
8 (*a*) C. M. Nelson and M. J. Bissell, *Annu. Rev. Cell Dev. Biol.*, 2006, **22**, 287; (*b*) R. Xu, A. Boudreau and M. Bissell, *Cancer Metastasis Rev.*, 2009, **28**, 167.
9 (*a*) C. Moraes, Y. Sun and C. A. Simmons, *Integr. Biol.*, 2011, **3**, 959; (*b*) D. H. Kim, P. K. Wong, J. Park, A. Levchenko and Y. Sun, in *Annu. Rev. Biomed. Eng.*, Annual Reviews: Palo Alto, 2009, vol. 11, pp. 203–233; (*c*) D. E. Ingber, *Int. J. Dev. Biol.*, 2006, **50**, 255.
10 (*a*) C. S. Chen, M. Mrksich, S. Huang, G. M. Whitesides and D. E. Ingber, *Science*, 1997, **276**, 1425; (*b*) C. M. Nelson, R. P. Jean, J. L. Tan, W. F. Liu, N. J. Sniadecki, A. A. Spector and C. S. Chen, *Proc. Natl. Acad. Sci. U. S. A.*, 2005, **102**, 11594; (*c*) K. A. Kilian, B. Bugarija, B. T. Lahn and M. Mrksich, *Proc. Natl. Acad. Sci. U. S. A.*, 2010, **107**, 4872.
11 (*a*) T. Gudjonsson, L. Ronnov-Jessen, R. Villadsen, M. J. Bissell and O. W. Petersena, *Methods*, 2003, **30**, 247; (*b*) M. J. Bissell, A. Rizki and I. S. Mian, *Curr. Opin. Cell Biol.*, 2003, **15**, 753; (*c*) G. Y. Lee, P. A. Kenny, E. H. Lee and M. J. Bissell, *Nat. Methods*, 2007, **4**, 359.
12 N. Gjorevski and C. M. Nelson, *Integr. Biol.*, 2010, **2**, 424.
13 E. W. Gomez, Q. K. Chen, N. Gjorevski and C. M. Nelson, *J. Cell. Biochem.*, 2010, **110**, 44.
14 (*a*) S. A. Ruiz and C. S. Chen, *Stem Cells*, 2008, **26**, 2921; (*b*) L. Gao, R. McBeath and C. S. Chen, *Stem Cells*, 2010, **28**, 564.
15 C. M. Nelson, J. L. Inman and M. J. Bissell, *Nat. Protocols*, 2008, **3**, 674.
16 (*a*) M. Nikkhah, F. Edalat, S. Manoucheri and A. Khademhosseini, *Biomaterials*, 2012, **33**, 5230; (*b*) O. Z. Fisher, A. Khademhosseini, R. Langer and N. A. Peppas, *Acc. Chem. Res.*, 2010, **43**, 419.
17 (*a*) D. R. Albrecht, V. L. Tsang, R. L. Sah and S. N. Bhatia, *Lab Chip*, 2005, **5**, 111; (*b*) D. R. Albrecht, G. H. Underhill, T. B. Wassermann, R. L. Sah and S. N. Bhatia, *Nat. Methods*, 2006, **3**, 369.
18 R. J. Mason, *Respirology*, 2006, **11**, S12.
19 C. A. DeForest and K. S. Anseth, *Nat. Chem.*, 2011, **3**, 925.
20 (*a*) C. P. Holmes, *J. Org. Chem.*, 1997, **62**, 2370; (*b*) J. A. Johnson, J. M. Baskin, C. R. Bertozzi, J. T. Koberstein and N. J. Turro, *Chem. Commun.*, 2008, 3064; (*c*) M. Alvarez, A. Best, S. Pradhan-Kadam, K. Koynov, U. Jonas and M. Kreiter, *Adv. Mater.*, 2008, **20**, 4563; (*d*) Y. R. Zhao, Q. Zheng, K. Dakin, K. Xu, M. L. Martinez and W. H. Li, *J. Am. Chem. Soc.*, 2004, **126**, 4653; (*e*) D. Y. Wong, D. R. Griffin, J. Reed and A. M. Kasko, *Macromolecules*, 2010, **43**, 2824; (*f*) A. M. Kloxin, A. M. Kasko, C. N. Salinas and K. S. Anseth, *Science*, 2009, **324**, 59; (*g*) A. M. Kloxin, M. W. Tibbitt and K. S. Anseth, *Nat. Protocols*, 2010, **5**, 1867.
21 (*a*) M. P. Lutolf, J. L. Lauer-Fields, H. G. Schmoekel, A. T. Metters, F. E. Weber, G. B. Fields and J. A. Hubbell, *Proc. Natl. Acad. Sci. U. S. A.*, 2003, **100**, 5413; (*b*) B. D. Fairbanks, M. P. Schwartz, A. E. Halevi, C. R. Nuttelman, C. N. Bowman and K. S. Anseth, *Adv. Mater.*, 2009, **21**, 5005; (*c*) J. Patterson and J. A. Hubbell, *Biomaterials*, 2010, **31**, 7836; (*d*) H. Nagase and G. B. Fields, *Biopolymers*, 1996, **40**, 1996.
22 C. A. DeForest, B. D. Polizzotti and K. S. Anseth, *Nat. Mater.*, 2009, **8**, 659.
23 (*a*) D. M. Walba, C. A. Liberko, E. Korblova, M. Farrow, T. E. Furtak, B. C. Chow, D. K. Schwartz, A. S. Freeman, K. Douglas, S. D. Williams, A. F. Klittnick and N. A. Clark, *Liq. Cryst.*, 2004, **31**, 481; (*b*) B. J. Adzima, Y. H. Tao, C. J. Kloxin, C. A. DeForest, K. S. Anseth and C. N. Bowman, *Nat. Chem.*, 2011, **3**, 256.
24 H. A. Simms, C. A. Bowman and K. S. Anseth, *Biomaterials*, 2008, **29**, 2228.
25 (*a*) A. M. Kloxin, M. W. Tibbitt, A. M. Kasko, J. F. Fairbairn and K. S. Anseth, *Adv. Mater.*, 2010, **22**, 61; (*b*) M. W. Tibbitt, A. M. Kloxin, K. U. Dyamenahalli and K. S. Anseth, *Soft Matter*, 2010, **6**, 5100.
26 A. E. Rydholm, S. K. Reddy, K. S. Anseth and C. N. Bowman, *Polymer*, 2007, **48**, 4589.
27 (*a*) P. J. Flory and J. Rehner, *J. Chem. Phys.*, 1943, **11**, 512; (*b*) P. J. Flory, *Principles of Polymer Chemistry*, Cornell University, 1953, p. 672.
28 A. B. Bernard, C. C. Lin and K. S. Anseth, *Tissue Eng.*, 2012, **18**, 1.
29 (*a*) T. Yano, R. J. Mason, T. L. Pan, R. R. Deterding, L. D. Nielsen and J. M. Shannon, *Am. J. Physiol.: Lung Cell. Mol. Physiol.*, 2000, **279**, L1146; (*b*) W. Y. Park, B. Miranda, D. Lebeche, G. Hashimoto and W. V. Cardoso, *Dev. Biol.*, 1998, **201**, 125.
30 A. Pardo, K. Ridge, B. Uhal, J. Iasha Sznajder and M. Selman, *Int. J. Biochem. Cell Biol.*, 1997, **29**, 901.
31 G. P. Raeber, M. P. Lutolf and J. A. Hubbell, *Biophys. J.*, 2005, **89**, 1374.
32 S. B. Anderson, C. C. Lin, D. V. Kuntzler and K. S. Anseth, *Biomaterials*, 2011, **32**, 3564.
33 J. A. Benton, B. D. Fairbanks and K. S. Anseth, *Biomaterials*, 2009, **30**, 6593.
34 M. Ehrbar, A. Sala, P. Lienemann, A. Ranga, K. Mosiewicz, A. Bittermann, S. C. Rizzi, F. E. Weber and M. P. Lutolf, *Biophys. J.*, 2011, **100**, 284.
35 B. K. Mann, A. S. Gobin, A. T. Tsai, R. H. Schmedlen and J. L. West, *Biomaterials*, 2001, **22**, 3045.
36 C. A. DeForest, E. A. Sims and K. S. Anseth, *Chem. Mater.*, 2010, **22**, 4783.
37 C. A. DeForest and K. S. Anseth, *Angew. Chem., Int. Ed.*, 2011, **51**, 1816.
38 M. C. Williams, *Annu. Rev. Physiol.*, 2003, **65**, 669.
39 M. J. Mondrinos, S. Koutzaki, E. Jiwanmall, M. Y. Li, J. P. Dechadarevian, P. I. Lelkes and C. M. Finck, *Tissue Eng.*, 2006, **12**, 717.
40 M. Ochs, L. R. Nyengaard, A. Lung, L. Knudsen, M. Voigt, T. Wahlers, J. Richter and H. J. G. Gundersen, *Am. J. Respir. Crit. Care Med.*, 2004, **169**, 120.
41 A. Tsuda, N. Filipovic, D. Haberthur, R. Dickie, Y. Matsui, M. Stampanoni and J. C. Schittny, *J. Appl. Physiol.*, 2008, **105**, 964.
42 E. L. Herzog, A. R. Brody, T. V. Colby, R. J. Mason and M. C. Williams, *Proc. Am. Thorac. Soc.*, 2008, **5**, 778.
43 H. Fehrenbach, *Respir. Res.*, 2001, **2**, 33.
44 S. Bellusci, J. Grindley, H. Emoto, N. Itoh and B. L. M. Hogan, *Development*, 1997, **124**, 4867.